Detectability of Changes in the Walker Circulation in Response to Global Warming*

PEDRO N. DINEZIO

International Pacific Research Center, School of Ocean and Earth Science and Technology, University of Hawaii at Manoa, Honolulu, Hawaii

GABRIEL A. VECCHI

NOAA/Geophysical Fluid Dynamics Laboratory, Princeton, New Jersey

AMY C. CLEMENT

Rosenstiel School of Marine and Atmospheric Science, University of Miami, Miami, Florida

(Manuscript received 29 July 2012, in final form 10 December 2012)

ABSTRACT

Changes in the gradients in sea level pressure (SLP) and sea surface temperature (SST) along the equatorial Pacific are analyzed in observations and 101 numerical experiments performed with 37 climate models participating in the fifth phase of the Coupled Model Intercomparison Project (CMIP5). The ensemble of numerical experiments simulates changes in the earth's climate during the 1870–2004 period in response to changes in natural (solar variations and volcanoes) and anthropogenic (well-mixed greenhouse gases, ozone, direct aerosol forcing, and land use) radiative forcings. A reduction in the zonal SLP gradient is present in observational records and is the typical response of the ensemble, yet only 26 out of the 101 experiments exhibit a reduced SLP gradient within 95% statistical confidence of the observed value. The multimodel response indicates a reduction of the Walker circulation to historical forcings, albeit an order of magnitude smaller than the observed value. There are multiple nonexclusive interpretations of these results: (i) the observed trend may not be entirely forced and includes a substantial component from internal variability; (ii) there are problems with the observational record that lead to a spuriously large trend; and (iii) the strength of the Walker circulation, as measured by the zonal SLP gradient, may be less sensitive to external forcing in models than in the real climate system. Analysis of a subset of experiments suggests that greenhouse gases act to weaken the circulation, but aerosol forcing drives a strengthening of the circulation, which appears to be overestimated by the models, resulting in a muted response to the combined anthropogenic forcings.

1. Introduction

Observations exhibit a reduction in the east–west contrast in sea level pressure (SLP) along the equatorial Pacific during the twentieth century (Vecchi et al. 2006; Zhang and Song 2006; Power and Smith 2007; Karnauskas et al. 2009; DiNezio et al. 2010) (Fig. 1). This trend reflects a weakening of the Walker circulation: the large-scale zonal flow of air with upward motion over the Maritime Continent and subsidence over the central and eastern Pacific Ocean. This weakening of the Walker circulation was first attributed by Vecchi et al. (2006, hereafter V06) using an ensemble of five numerical experiments performed with the GFDL CM2.1. The spatial pattern and magnitude of the SLP trends observed over the tropical Indo-Pacific during 1861–1992 agree with the simulated changes, only when the model is forced with anthropogenic changes in radiative forcings. This response is also a robust feature of global warming simulations for the twenty-first century, where the

* School of Ocean and Earth Science and Technology Publication Number 8813 and International Pacific Research Center Publication Number 939.

Corresponding author address: Pedro N. DiNezio, International Pacific Research Center, School of Ocean and Earth Science and Technology, University of Hawaii at Manoa, Honolulu, HI 96822.
E-mail: pdn@hawaii.edu

DOI: 10.1175/JCLI-D-12-00531.1

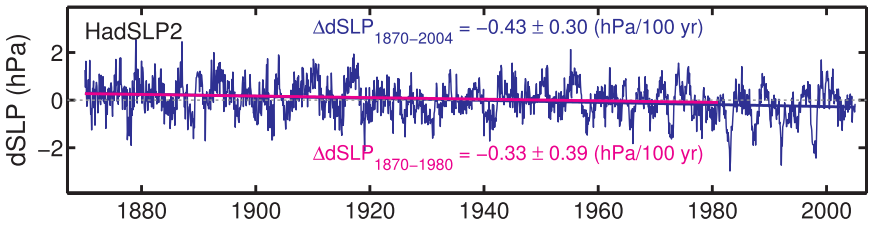

FIG. 1. Observed time series of zonal equatorial gradient in sea level pressure dSLP during the 1870 to 2004 period (HadSLP2 dataset). The SLP gradient dSLP is a measure of the strength of the Walker circulation. The dSLP time series is computed as the area average of the monthly SLP fields over a Tahiti region (5°S–5°N, 160°–80°W) minus a Darwin region (5°S–5°N, 100°E–180°). The error bar of the trends are given by the 95% confidence interval computed using a Student's *t* distribution with reduced degrees of freedom to account for autocorrelation in the time series.

ascending branch of the Walker circulation weakens in order to maintain a balanced transport of water vapor in areas of convection, as precipitation increases in response to surface warming at a smaller rate than humidity (Held and Soden 2006; Vecchi and Soden 2007). This differential in the rates of change of humidity and precipitation has not been detected in observations, though the length and quality of the observational record may be insufficient to constrain the response of global precipitation (Chou and Neelin 2004; Wentz et al. 2007; Liepert and Previdi 2009).

The detection and attribution of the externally forced weakening of the Walker circulation can be confounded by the very large internal variability of the tropical Pacific (V06; Deser et al. 2010b; Power and Kociuba 2011). For instance, the observed SLP trends exhibit a large reversal since the 1990s with stronger trade winds and Walker circulation (Merrifield 2011). Conversely, the largest multidecadal weakening of the Walker circulation occurred during the 1977–2006 period coincident with an increase in the frequency of El Niño and a reduction in the frequency of La Niña (Power and Smith 2007). Previous studies have estimated a wide range of detection time scales from 60 (Tokinaga et al. 2012b) to 130 yr (V06).

Are natural internally generated changes in the Walker circulation masking the forced signal due to global warming? Sensitivity to warming and the magnitude of the internal variability differ from model to model; thus, the detectability of the forced changes is likely to be model dependent. To overcome this issue, Power and Kociuba (2011) analyzed SLP trends simulated by a multimodel ensemble of simulations of the twentieth-century climate coordinated by phase 3 of the Coupled Model Intercomparison Project (CMIP3). Their results suggest that the observed SLP trends during the twentieth century are due to a combination of both unforced internal climate variability and greenhouse gas (GHG)–forced global warming.

Here we address these questions comparing trends in SLP and SST observations with 101 ''historical'' experiments performed with 37 climate models participating in the phase 5 of the Coupled Model Intercomparison Project (CMIP5). Note that the attribution study done by V06 relied on an ensemble of five simulations using one single model, GFDL CM2.1. Deser et al. (2010b) used the CCSM3.0 to show that ensembles of at least 20 simulations are required to isolate forced changes in tropical circulation in response to twenty-first-century forcings. Power and Kociuba (2011) used a multimodel ensemble of twentieth-century climate simulations coordinated by CMIP3. Here we apply their methodology to a much larger ensemble of twentieth-century climate simulations coordinated by CMIP5. We look at each model's range of simulated changes in order to determine whether the forced weakening of the Walker circulation is already detectable in the modern observational record. To conclude, we use a subset of new CMIP5 experiments, where the models are forced solely with each type of forcing, to explore how the different anthropogenic and natural forcings could drive changes in the Walker circulation.

2. Model and observational data

We use observed and simulated SLP and SST data to detect and attribute changes in the strength of the Walker circulation during the 1870–2004 period and its relationship with patterns of warming. The observed data are monthly-mean SLP fields from the Second Hadley Centre Sea Level Pressure dataset (HadSLP2; Allan and Ansell 2006) and monthly-mean SST fields from the extended reconstructed SST, version 3 (ERSST3) dataset (Smith et al. 2008) and Hadley Centre Sea Ice and Sea Surface Temperature dataset (HadISST; Rayner et al. 2003). The simulated data consists of monthly-mean SLP and SST fields from an ensemble of 104 historical experiments coordinated by CMIP5 and

performed with 37 different coupled climate models. These historical experiments simulate changes in Earth's climate during the 1850–2005 period in response to changes in natural (solar variations and volcanoes) and anthropogenic (well-mixed greenhouse gases, ozone, direct aerosol forcing, and land use) radiative forcings. We also use an ensemble of 31 historical experiments performed with 7 different models forced solely with GHG or natural forcing (historicalGHG and historicalNat in the CMIP5 archive) to explore the origin of the SLP trends.

We estimate the variability and change in the east–west SLP gradient along the equatorial Pacific Ocean both from observations and each simulation. For this we use the dSLP index defined by V06 as the difference of the area averaged SLP between a ''Tahiti'' region (5°S–5°N, 160°–80°W) minus a ''Darwin'' region (5°S–5°N, 100°E–180°). This index measures changes in the zonal SLP gradient along the equatorial Pacific, a proxy for the strength of the Walker circulation. We also define a dSST index as the difference of the area-averaged SST between the Tahiti and Darwin regions to explore the relationship between changes in the SST gradient and the Walker circulation.

Most CMIP5 historical experiments begin in 1850, and a few others begin in 1860. The HadISST and ERSST3 datasets start in 1870, and the HadSLP2 record starts in 1860. All observational datasets extend until 2004. There is a near-real-time SLP dataset (HadSLP2r) that extends until 2012, but the variance in the HadSLP2r is larger after 2005, potentially introducing spurious trends (see next subsection). For these reasons, we focus on the 1870–2004 period when all three observational datasets and historical simulations have coinciding data. The changes in the dSLP and dSST indices are computed as least squares linear trends in each individual historical experiment over 1870–2004. We also explore the detectability of the trends during shorter periods beginning from 1870 to 1970, all ending in 2004.

Issues with SLP datasets after 2005

This study could be extended until 2012 using an extension of the historical experiment (historicalExt) or any of the emission scenario experiments (rcp45, rcp60, rcp85) coordinated by CMIP5, along with the HadSLP2r dataset for observed changes. The HadSLP2r dataset is an extended HadSLP2 dataset in which SLP fields from the National Centers for Environmental Prediction–National Center for Atmospheric Research (NCEP–NCAR) reanalysis (Kalnay et al. 1996) are appended to the HadSLP2 dataset after 2004, to allow analyses to the present. The HadSLP2 dataset (Allan and Ansell 2006) is a spatially complete dataset of SLP from 1860–2004, in which a consistent methodology was applied to sparse observations to generate global reconstructions of SLP, and therefore suitable for climate applications. The HadSLP2r is widely used for climate applications, even though it is a concatenation of two disparate datasets. After exploring the character of the HadSLP2r SLP evolution (Fig. 2), we have decided against using it, since it includes a spurious shift in its variance characteristics that impacts trends and other estimates of multidecadal to centennial change. The inhomogeneity of HadSLP2r across the 2004–05 data splice is also likely to be problematic for many other applications: the bottom panels in Fig. 2 focus on the impact to near-equatorial Pacific SLP, but comparable impacts are seen throughout the globe.

The real-time extension of HadSLP2 is done by appending SLP values from the NCEP reanalysis to HadSLP2; the NCEP data are correlated only for the mean differences in SLP between HadSLP2 and NCEP over the overlapping period. However, HadSLP2 is a reconstruction from a sparse data network, a property of which is to reduce the variance of the overall anomalies thus to recover a consistent reconstruction over the entire record. Meanwhile, NCEP is a model-based reanalysis, which does not aim to reduce variance. Therefore, though the mean differences between the two products are corrected, differences in the variance are not. As can be seen in Fig. 2, starting in 2005, the character of anomalies in HadSLP2r changes markedly. Therefore, HadSLP2r cannot be treated as a climate data record to explore changes in the character of SLP across the 2004–05 boundary.

3. Detection and attribution of the observed changes

There is clear evidence from previous studies that the dSLP trends in each individual experiment include both forced and unforced changes. Multidecadal trends due to unforced internal variability are likely to dominate the trends during periods shorter than 100 yr (V06). We address these issues by computing the multimodel ensemble mean (MMEM) and the probability density function (PDF) of the dSLP trends for a range of detections periods ending on 2004, but starting sequentially from 1870 every 10 yr until 1980. Figure 3 shows the MMEM (solid white line) and the PDF (colors) of the dSLP trends (y axis) as a function of the start date of the detection period (x axis). The ensemble of historical experiments analyzed here provides 101 independent realizations of climate that we use in the estimation of the MMEM and PDF of the trends. Trends due to random unforced variability cancel out in the averaging, resulting

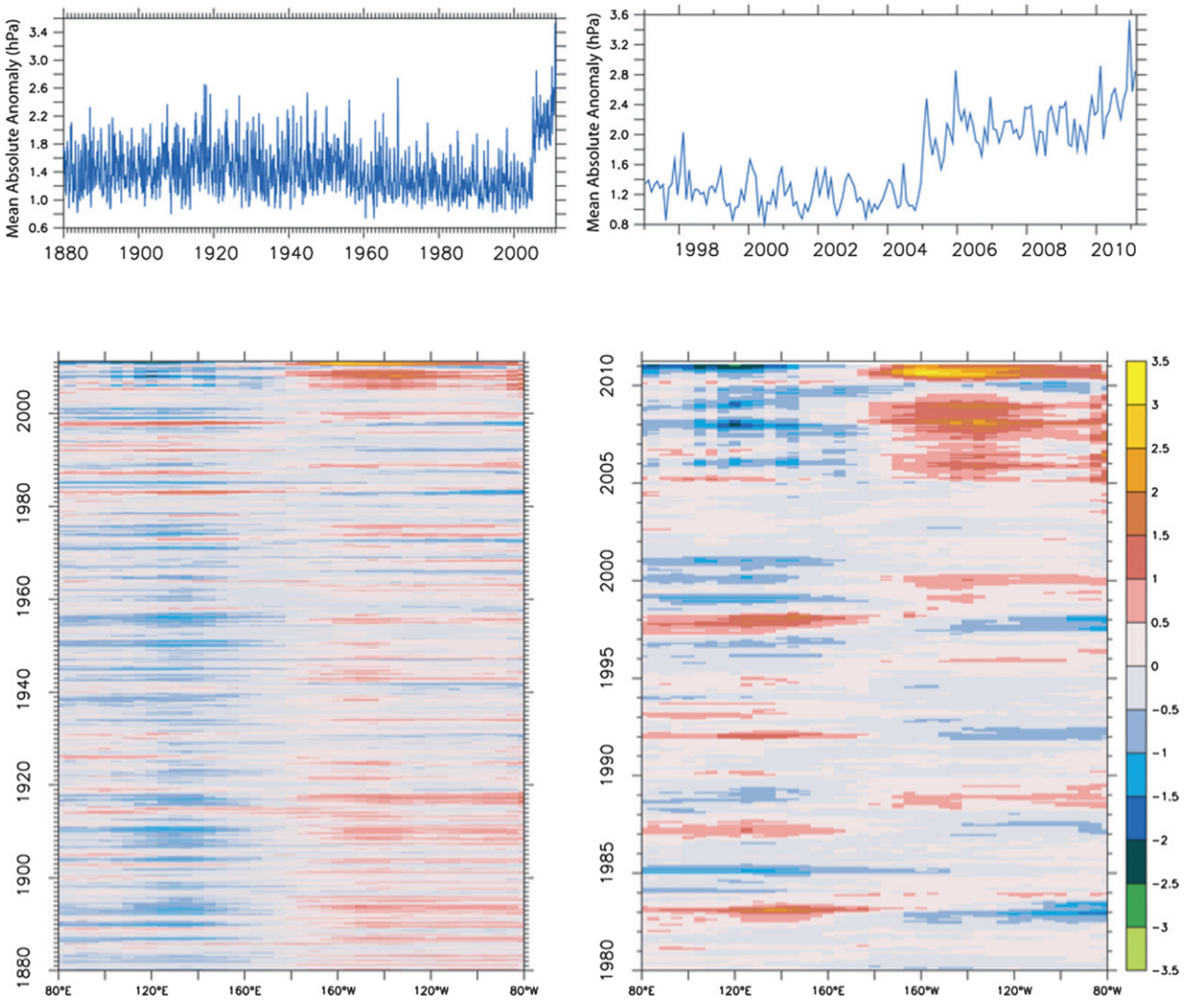

FIG. 2. Impact of the extension of HadSLP2 past 2004 in the HadSLP2r dataset. (top) Time series of the global mean of the absolute value of SLP anomaly (relative to the 1880–2004 average) with (right) focus on the end of the record. Notice the change in the amplitude of the typical SLP anomalies coincident with the switch in 2004 between HadSLP2 (Allan and Ansell 2006) and HadSLP2r (real-time updates); the typical anomalies are almost twice as large for 2005–11 as prior to that. (bottom) Hovmöller plots of near-equatorial Pacific seasonally smoothed SLP anomaly: (right) focus on the end of the record in (left). Notice how the anomalies starting in 2005 are unprecedented, exceeding even the extreme La Niña of 1998/99 or the largest El Niños on record (1982/83 and 1997/98).

in a MMEM trend that estimates the magnitude of the forced response. Conversely, the PDF characterizes the possible trend values associated with differences in model physics, as well as random internal variability. The PDFs for each detection period are computed using the kernel density estimation method (Parzen 1962). Note that long-term trends due to internal (i.e., unforced) variability are also random, since each simulation is initialized from different initial conditions and their climate evolves following a distinct trajectory. The MMEM averages these internally generated long-term trends out, since they uncorrelated among simulations, isolating the forced response, which is common to all simulations.

The MMEM dSLP trend has a magnitude of -0.05 ± 0.33 hPa $(100\ \text{yr})^{-1}$ during the 1870–2004 period, indicating a weakening of the SLP gradient (Fig. 3, white line). The error of the MMEM dSLP reflects the 95% confidence interval derived from the 101 simulated dSLP trends. The magnitude of this weakening increases slowly for shorter detection periods, reaching a value of -0.13 ± 0.96 hPa $(100\ \text{yr})^{-1}$ for the 1960–2004 period. Conversely, The PDF of the dSLP trends widens as the detection period shortens (Fig. 3, shading). However,

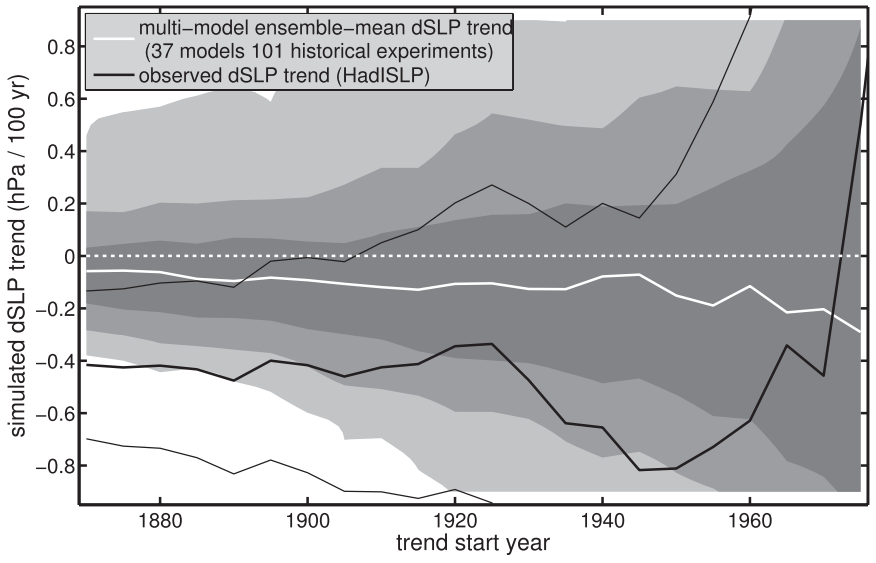

FIG. 3. Probability of the simulated dSLP trends as a function of detection period computed using the ensemble of 101 historical experiments. Shadings show the 0.5% (3σ), 2.5% (2σ), and 16.5% (1σ) percentile ranges from lighter to darker gray so that the shaded area covers 99%, 95%, and 66% of the trends, respectively. See Fig. 1 or section 2 for details on the computation of dSLP index. The detection periods begin at different years from 1870 to 1980 (x axis) all ending in 2004. The solid white line is the multimodel ensemble-mean trend dSLP trends for each detection period. The solid black line is the observed trend for each detection period. The thin black lines delimit the 95% confidence interval of the observed trends computed from Student's t distribution with reduced degrees of freedom accounting for autocorrelation in the dSLP index.

even for the 1870–2004 detection period, a substantial fraction of the trends (25%) are positive, indicating that the Walker circulation strengthens in these models. The PDF of the dSLP trends becomes nearly uniform for detection periods beginning in 1970. This indicates that a wide range of positive or negative trends are equally likely, despite the fact that the MMEM trend (i.e., the forced trend) is nonzero. For longer detection periods beginning from 1870 to 1950, the spread of the simulated dSLP trends appears to be dominated by intermodel differences in the magnitude of the forced response, with internal variability playing a lesser role. Figure 3 shows that the spread among the simulations becomes larger for shorter detection periods; this is because internal variability dominates in the dSLP trends. However, the MMEM remains relatively steady around the 1870–2004 MMEM dSLP trend with some tendency toward ever more negative values, possibly due to accelerating radiative forcing toward the end of the twentieth century. This suggests that because of the large size of our ensemble, the MMEM captures the forced response for shorter detection periods as well.

In contrast, the magnitude of the observed dSLP trend during the 1870–2004 period is -0.43 ± 0.30 hPa $(100\ \text{yr})^{-1}$. The error bars of the trends are given by the 95% confidence interval computed using a Student's t distribution with reduced degrees of freedom to account for autocorrelation in the dSLP time series. Similar trend values are obtained from detection periods starting in 1870 through 1920. The magnitude of the observed dSLP trend is not only much larger than the MMEM value of -0.05 ± 0.33 hPa $(100\ \text{yr})^{-1}$ (Fig. 3, black line) but also unlikely to occur in response to changes in forcing, according to the multimodel PDF. In fact, there are only 26 experiments (out of 101) that simulate dSLP trends within the 95% confidence limits of the observed dSLP trend.

What is the contribution of forced and unforced variability to the observed trend? To answer this question we compute the ensemble-mean (EM) dSLP and dSST trends for those models with more than one historical experiment. We also expect that each model's EM will capture the magnitude of the forced trend. In this analysis, we include the dSST trends in order to explore the role of patterns in warming in the response of the Walker circulation. Note that none of the models has run up to 20 ensemble members required to isolate forced trends (Deser et al. 2010b). Thus, we also estimate the range of trends simulated by each model in the different experiments as an estimate of the uncertainty

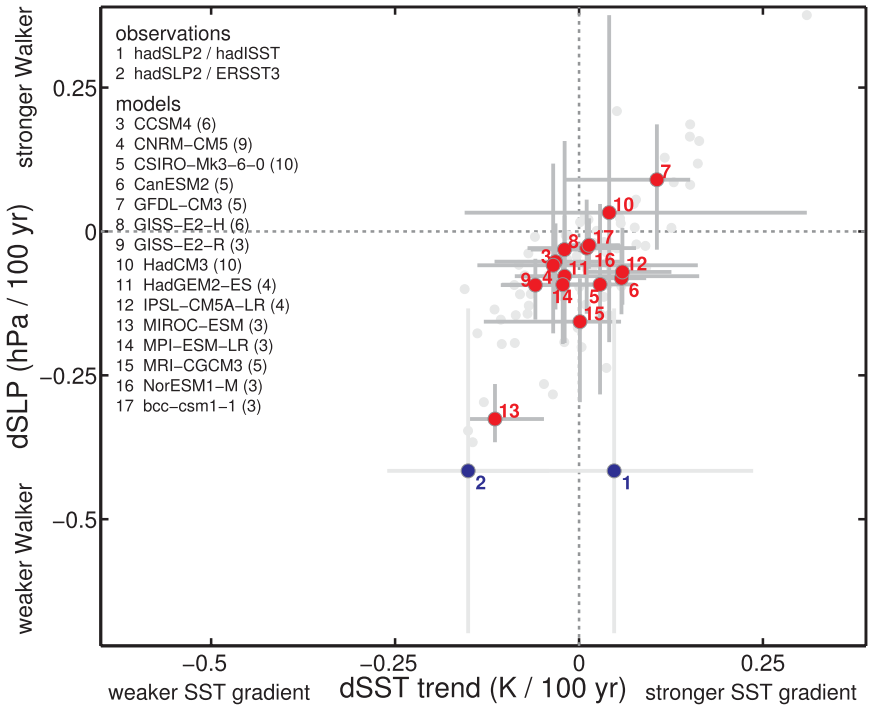

FIG. 4. Linear trends in the east–west equatorial gradients of sea surface temperature dSST and sea level pressure dSLP during the 1870 to 2004 period in observations (blue) and in CMIP5 historical experiments (red). The SLP gradient dSLP is a measure of the strength of the Walker circulation. See Fig. 1 or section 2 for details on the dSLP and dSST indices. The red dots are the ensemble-mean trend for each model and the error bars show the spread among the trends simulated by the model in each experiment. The error bars are the maximum–minimum values of the dSLP and dSST trends. The gray dots are the trends from each individual experiment. Only changes simulated by models with more than one historical experiment are shown. The number along with the model name indicates the number of runs of the historical experiment by each model. The error bars of the observed trends are given by the 95% confidence interval computed using a Student's t distribution with reduced degrees of freedom to account for autocorrelation in the time series.

because of internal variability. These estimates of the range of unforced trends include the effect of ENSO variability, since periods with enhanced ENSO variability rectify into warm decadal climate anomalies due to the asymmetry between warm and cold events (Newman et al. 2003; Rodgers et al. 2004; Vimont 2005), as well as the effect of other sources of decadal climate.

A total of 12 models simulate EM dSLP trends that are negative over the 1870–2004 period (Fig. 4a, red dots, y axis). However, some of the individual experiments simulate positive dSLP trends, despite the fact that respective EM trends are negative (e.g., CNRM-CM5, CSIRO Mk3.6.0, CanESM2, IPSL-CM5A-LR, HadGEM2-ES; model expansions are provided in Table 1). These models suggest that unforced century-time-scale trends can overwhelm the forced signals. Only five models (CanESM2, GISS-E2-R, MIROC-ESM, MPI-ESM-LR, and MRI-CGCM3) simulate a detectable weakening of the Walker circulation; that is, all the experiments performed with these models simulate negative dSLP trends (Fig. 4, dots 9, 13, and 5).

Because of the strong coupling between equatorial SST and SLP gradients (Bjerknes 1969), one would expect that models with a weaker Walker circulation would simulate a weaker SST gradient. However, not all the models that simulate a weakening of the Walker circulation (EM dSLP trend < 0) simulate a weakened east–west sea surface temperature gradient (EM dSST trend < 0) (Fig. 4, red dots, x axis). This could occur because the weakening of the Walker circulation is driven by changes in the hydrological cycle driving that are governed by the magnitude of tropical-mean warming, even in the absence of patterns of warming. Conversely, the boxes used to compute dSST might not be optimally located to capture the changes that are relevant for each particular model. We explored several

TABLE 1. Model expansions.

Model	Expansion
CanESM2	Canadian Earth System Model, version 2
CCSM	Community Climate System Model
CMIP	Coupled Model Intercomparison Project
CNRM-CM5	Centre National de Recherches Météorologiques Coupled Global Climate Model, version 5
CSIRO Mk3.6.0	Commonwealth Scientific and Industrial Research Organisation Mark, version 3.6.0
GFDL CM2.1	Geophysical Fluid Dynamics Laboratory Climate Model version 2.1
GISS-E2-R	Goddard Institute for Space Studies Model E2-R
HadCM3	Third climate configuration of the Met Office Unified Model
HadGEM2-ES	Hadley Centre Global Environmental Model 2, Earth System
IPSL-CM5A-LR	L'Institut Pierre-Simon Laplace Coupled Model, version 5, coupled with NEMO, low resolution
MIROC-ESM	Model for Interdisciplinary Research on Climate, version 5, Earth System Model
MPI-ESM-LR	Max Planck Institute Earth System Model, low resolution
MRI-CGCM3	Meteorological Research Institute Coupled General Circulation Model, version 3

definitions of the zonal SST gradient, and none of them shows a clear relationship with the SLP gradient.

In general, however, the changes in dSST appear to play a role weakening the Walker circulation because the models with weaker dSST simulate the largest weakening in dSLP (e.g., MIROC-ESM). Conversely, the models that simulate stronger Walker circulations tend to simulate a stronger SST gradient (dSST trend > 0) (e.g., GFDL CM3). An alternative explanation is that even for periods as long as 1870–2004, the individual trends could still be dominated by internal variability in the tropical Pacific, which exhibits highly correlated changes in SLP and SST gradients since it arises from coupled ocean–atmosphere interactions. The high correlation ($r = 0.81$) between the dSLP and dSST trends of the individual experiments (Fig. 4, gray dots) supports this idea. The trends in ERSST3 agree well with the experiments with the largest dSLP and dSST trends (MIROC-ESM and MRI-CGCM3). In contrast, there is no experiment that simulates dSST and dSLP trends comparable to those than HadISST and HadSLP2.

Only 25 out of 101 experiments simulate dSLP trends within 95% statistical significance of the observed value. Furthermore, only two models (MIROC-ESM and MRI-CGCM3) simulate an EM dSLP change comparable with the observed value; thus, according to these two models, the observed trends would be entirely forced. Note that despite only three realizations were used to compute MIROC-ESM's EM trend, the weaker internal variability simulated by this model allows the forced response to dominate in all the simulations. Conversely, three out six simulations performed with MRI-CGCM3 exhibit a dSLP trend within 95% statistical significance of the observed value. Note that the EM trend of MRI-CGCM3 is -0.15 hPa $(100\ \text{yr})^{-1}$; thus, according to this model, the observed trend is about equal parts forced and unforced.

The remaining 26 simulations agreeing with the observations were performed by models with EM dSLP trends smaller than the observed value of -0.43 ± 0.30 $(100\ \text{yr})^{-1}$. Thus, according to these models, the observed dSLP trend is not 100% forced. One of these models, HadCM3, simulates a positive EM dSLP trend: that is, a stronger Walker circulation in response to the changes in external forcing. Thus, according to this model, the observed dSLP trend would originate entirely from internal unforced variability. However, the internal variability simulated by HadCM3, as measured by a standard deviation of the dSLP index of 1.06 hPa, is much stronger than the observed value of 0.67 hPa. Thus, it is very unlikely that the observed trend is entirely unforced.

The observed dSLP trend during 1870–2004 is often attributed to the very strong 1982 and 1997 El Niño events at the end of the record. However, the -0.43 ± 0.30 hPa $(100\ \text{yr})^{-1}$ trend during the entire 1870–2004 period (Fig. 1, magenta line), is not statistically different from the -0.33 ± 0.39 hPa $(100\ \text{yr})^{-1}$ trend during the 1870–1980 period, which excludes these large El Niño events (Fig. 1, magenta line).

Sensitivity to historical forcings

The smaller-than-observed sensitivity of the Walker circulation to historical forcing exhibited by the CMIP5 models may also have resulted from opposing responses to the natural and anthropogenic forcings included in the historical experiment. Analysis of historicalGHG experiments performed with a smaller set of models shows evidence for this explanation. Five out of seven models show a larger response in the dSLP gradient when forced solely by changes in GHG gases (Fig. 5). Note that the number of ensemble members may not be large enough to isolate the responses to the different forcing. However, the experiments performed with GFDL CM3, GISS-E2-H, GISS-E2-R, and CCSM4 exhibit dSLP trends in response to GHG-only forcing (Fig. 5, blue bars) that fall outside the minimum–maximum range of trends simulated in response to all forcings (Fig. 5, blue bars) or to natural forcings (Fig. 5, green).

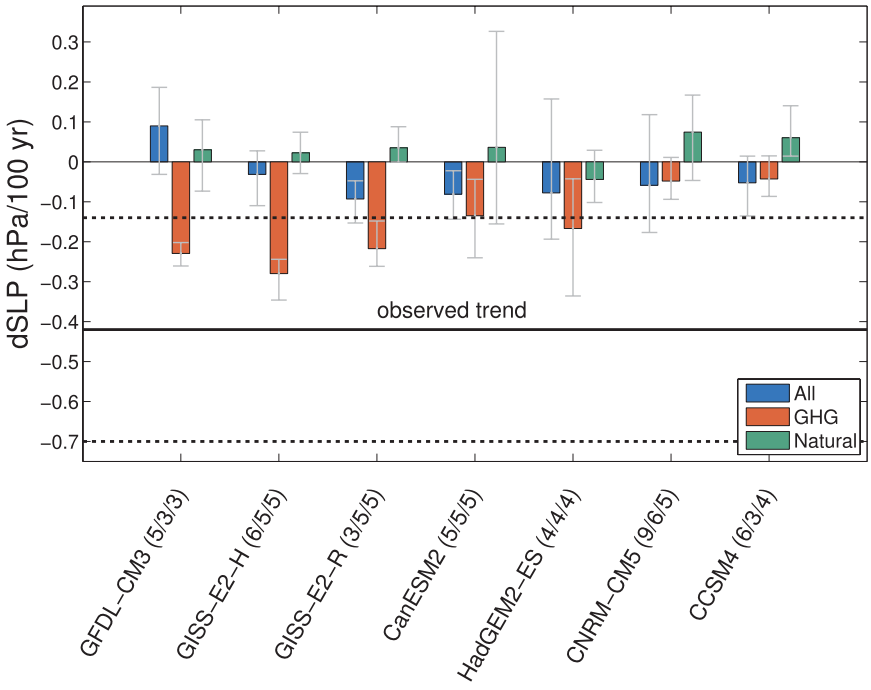

FIG. 5. Linear trends in the east–west sea level pressure gradient (dSLP) during the 1870–2004 period simulated by CMIP5 historical (blue), historicalGHG (red), and historicalNat (green) experiments. See Fig. 2 for details on how the dSLP index is computed. The bars are the EM trend simulated by each model. The error bars show the minimum–maximum range of the trends simulated the different experiments performed with each model. The number along with the model name indicates the number of experiments performed with each model. The solid black line is the observed trend with the dashed lines delimiting the 95% confidence interval of the observed trends computed from a Student's *t* distribution with reduced degrees of freedom accounting for autocorrelation in the dSLP index.

Note that aerosol forcing is only included in the historical simulations, but not in the historicalGHG or in the historicalNat. GHG forcing is included in the historical and in the historicalGHG simulations. Thus, assuming a linear response to the individual forcings, the response to aerosols can be estimated as the historical minus historicalGHG minus historicalNat changes in dSLP. The historical and historicalNat experiments simulate relatively similar dSLP changes (Fig. 5). Thus, the response to aerosols is roughly opposite to the response to GHGs (i.e., a strengthening of the Walker circulation).

The impact of each forcing on the changes in the Walker circulation is clearly shown by the shifts in the PDFs of the 1970–2004 dSLP trends (Fig. 6a). The PDF of the historicalNat experiments shows no tendency for changes in dSLP (green), while the PDF of the historicalGHG experiments shows a stronger sensitivity than to all historical forcing (natural and anthropogenic) combined (blue). The fact that the weakening of the Walker circulation to all historical forcing changes is smaller than to GHG forcing suggests that the anthropogenic aerosols, which are only included in the historical experiments, are acting to strengthen the circulation. The enhanced sensitivity to GHG forcing, however, does not prevent internal variability from overwhelming the forced trends on shorter periods, such as 1970–2004 (Fig. 6b), when 33% of the historicalGHG experiments still exhibit positive trends.

4. Discussion and conclusions

Analysis of 101 simulations of the climate of the 1870–2004 period coordinated by CMIP5 shows that the Walker circulation appears to be less sensitive to external forcing in models than in observations. The observed weakening of 0.43 ± 0.30 hPa $(100\ \text{yr})^{-1}$ agrees (within 95% statistical confidence) with the EM response of two models (MIROC-ESM and MRI-CGCM3). The remaining models, with at least one simulation agreeing with the observations, exhibit EM dSLP trends (i.e., forced responses) that are less than the observed value. In these experiments, the trends are due to a combination of forced and internal variability. Taken at face value, these experiments would suggest that both

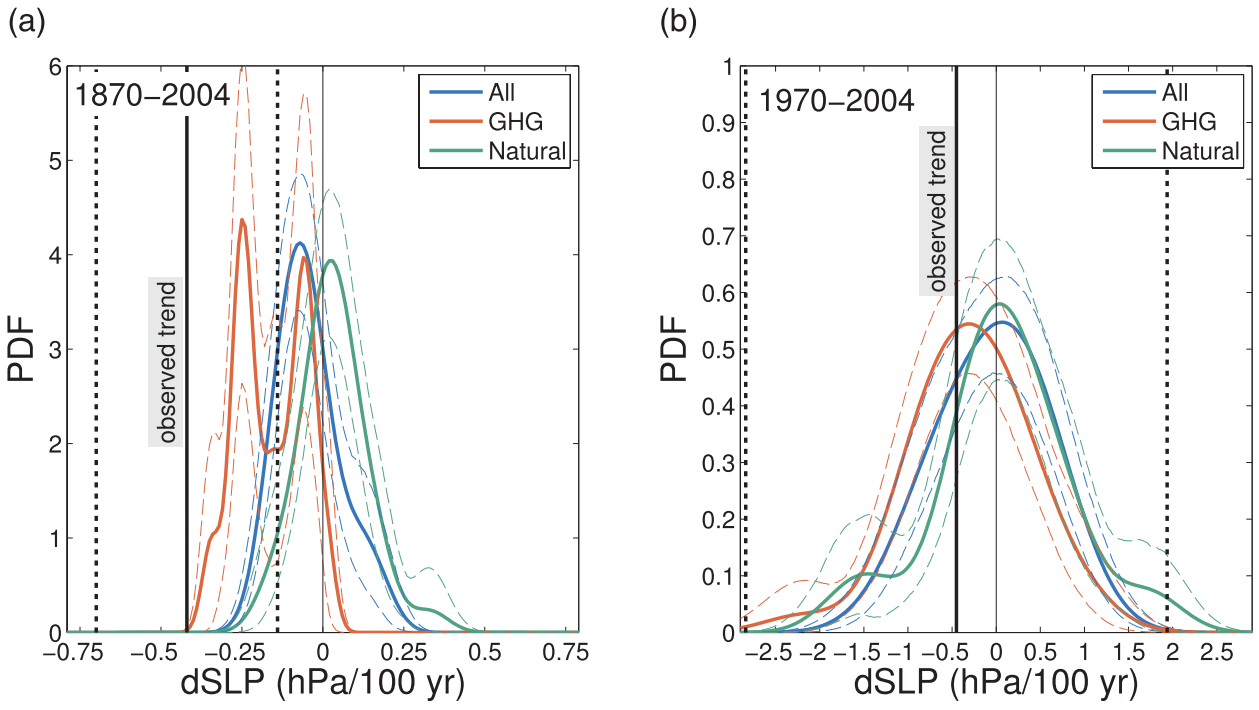

FIG. 6. Probability density function of the dSLP trends during (a) 1870–2004 and (b) 1970–2004 simulated in historical experiments forced solely with all (blue), anthropogenic greenhouse gas (red), and natural (green) forcings. The solid black line is the observed trend with the dashed lines delimiting the 95% confidence interval of the observed trends computed from a Student's *t* distribution with reduced degrees of freedom accounting for autocorrelation in the dSLP index. The dashed lines indicate the bootstrap 95% confidence interval of the PDFs.

natural and anthropogenic influences must be invoked to explain the observed trend and that the true sensitivity of the Walker circulation could be less than the observed trend in agreement with a previous study based on the CMIP3 archive (Power and Kociuba 2011).

The fact that the observed trend can only be explained by 26 out of 101 experiments could be pointing to issues in the models or the observations. The observed trend could be the result of spurious trends or biases, especially over ocean regions such as our equatorial Tahiti box, which have low data density before the 1940s (Allan and Ansell 2006). However, the 1877–2005 trend in SLP gradient has been estimated using data solely from the "Darwin" box, where coverage is more stable in time (Bunge and Clarke 2009). This method yields a 1877–2005 trend of -0.45 hPa $(100\ \text{yr})^{-1}$, which is virtually identical to the trend estimated from HadSLP2. On the other hand, the discrepancy between the model ensemble and observations could indicate that the Walker circulation in the models is not as sensitive to anthropogenic forcings as that in the real climate system. This conjecture is supported by a subset of models that show a weakening of the Walker circulation in response to GHG forcing closer to the observed value, which appears to be opposed by forcing by anthropogenic aerosols. We are currently exploring this issue with a more detailed experimental approach due to its relevance for attributing not only the observed centennial-scale trend but also the recent strengthening trend that has occurred in coincidence with the increase in aerosol forcing from Asia.

Evidence for a weaker Walker circulation is usually sought in the changes in the zonal SST gradient, because of the close relationship between dSLP and dSST on interannual and decadal time scales. However, the models do not show a reduction in dSST as robust as the weaker dSLP. We suggest that this is because the weakening of the Walker circulation is driven by changes in the hydrological cycle that are related not to changes in the SST gradient but to the magnitude of tropical-mean warming (Held and Soden 2006; Vecchi and Soden 2007; DiNezio et al. 2010). The different observational SST datasets show conflicting trends already reported by previous studies (Vecchi et al. 2008; Deser et al. 2010a). Recent studies show that the discrepancy among the SST datasets likely originates in changes in the observing system and the corrections applied to homogenize and combine bucket, engine

room water intake, satellite, and buoy measurements, as first hypothesized by Vecchi et al. (2008). HadISST exhibits a long-term cooling of the cold tongue and warming of the rest of the tropical Pacific resulting in a stronger dSST (Vecchi et al. 2008; Deser et al. 2010a).

Recent studies that carefully estimate warming patterns in the Pacific suggest that this cooling of the cold tongue maybe spurious. For instance, Bunge and Clarke (2009) used SLP observations to correct for sampling biases, which are pervasive in the equatorial Pacific before the 1950s to show that the Niño-3 region has warmed since 1880. This is consistent with Deser et al. (2010a), who find that the eastern equatorial Pacific has warmed both in nighttime marine air temperatures (NMAT), which follow SST by surface heat exchange, and in the HadSST2 dataset (a non-interpolated dataset). Tokinaga et al. (2012a) focus on the 1950–2009 period and show that bucket-sampled SSTs and NMAT also exhibit a weaker dSST. Moreover, the trends in ERSST3 agree well with the experiments with the largest dSLP and dSST trends (MIROC-ESM and MRI-CGCM3). This suggests that weakened SST gradients may play a role in a weakening of the SLP gradient with the observed magnitude.

Beginning in 1920 the observed trends show multidecadal variations, weakening down to -0.8 hPa $(100\ \text{yr})^{-1}$ during 1950–2004, even with a shift to positive trends (i.e., stronger Walker circulation) for trends beginning in 1970 [1.7 hPa $(100\ \text{yr})^{-1}$ during 1980–2004]. These trends are much different from the long-term trends of about -0.4 hPa $(100\ \text{yr})^{-1}$ computed from initial dates ranging from 1870 to 1920 and thus are likely to result from the multidecadal internal variability. Models also simulate a wide range of possible trends for detection periods beginning after the 1920s, thus confirming the results of V06 that records longer than 100 yr are required to detect changes in the Walker circulation. According to the models, it is very likely that changes detected in the tropical Pacific during the last 60 yr (e.g., Merrifield 2011; Tokinaga et al. 2012b) will be dominated by internal variability, reducing our ability to detect and attribute a forced trend in the recent part of the observation record.

Acknowledgments. We acknowledge the World Climate Research Programme's Working Group on Coupled Modelling, which is responsible for CMIP, and we thank the climate modeling groups for producing and making available their model output. For CMIP, the U.S. Department of Energy's Program for Climate Model Diagnosis and Intercomparison provides coordinating support and led development of software infrastructure in partnership with the Global Organization for Earth System Science Portals. P. N. DiNezio was supported by NSF (Grant AGS 1203754) and the University of Hawaii at Manoa. AC was supported by NSF (AGS0946225), NOAA (NA10OAR4310204), and DOE (DESC0004897).

REFERENCES

Allan, R., and T. Ansell, 2006: A new globally complete monthly historical gridded mean sea level pressure dataset (HadSLP2): 1850–2004. *J. Climate,* **19,** 5816–5842.

Bjerknes, J., 1969: Atmospheric teleconnections from the equatorial Pacific. *Mon. Wea. Rev.,* **97,** 163–172.

Bunge, L., and A. J. Clarke, 2009: A verified estimation of the El Niño index Niño-3.4 since 1877. *J. Climate,* **22,** 3979–3992.

Chou, C., and J. D. Neelin, 2004: Mechanisms of global warming impacts on regional tropical precipitation. *J. Climate,* **17,** 2688–2701.

Deser, C., A. S. Phillips, and M. A. Alexander, 2010a: Twentieth century tropical sea surface temperature trends revisited. *Geophys. Res. Lett.,* **37,** L10701, doi:10.1029/2010GL043321.

——, ——, V. Bourdette, and H. Teng, 2010b: Uncertainty in climate change projections: The role of internal variability. *Climate Dyn.,* **38,** 527–546, doi:10.1007/s00382-010-0977-x.

DiNezio, P. N., A. C. Clement, and G. A. Vecchi, 2010: Reconciling differing views of tropical Pacific climate change. *Eos, Trans. Amer. Geophys. Union,* **91,** 141–142.

Held, I. M., and B. J. Soden, 2006: Robust responses of the hydrological cycle to global warming. *J. Climate,* **19,** 5686–5699.

Kalnay, E., and Coauthors, 1996: The NCEP/NCAR 40-Year Reanalysis Project. *Bull. Amer. Meteor. Soc.,* **77,** 437–471.

Karnauskas, K. B., R. Seager, A. Kaplan, Y. Kushnir, and M. A. Cane, 2009: Observed strengthening of the zonal sea surface temperature gradient across the equatorial Pacific Ocean. *J. Climate,* **22,** 4316–4321.

Liepert, B. G., and M. Previdi, 2009: Do models and observations disagree on the rainfall response to global warming? *J. Climate,* **22,** 3156–3166.

Merrifield, M. A., 2011: A shift in western tropical Pacific sea level trends during the 1990s. *J. Climate,* **24,** 4126–4138.

Newman, M., G. P. Compo, and M. A. Alexander, 2003: ENSO-forced variability of the Pacific decadal oscillation. *J. Climate,* **16,** 3853–3857.

Parzen, E., 1962: On estimation of a probability density function and mode. *Ann. Math. Stat.,* **33,** 1065–1076.

Power, S. B., and I. N. Smith, 2007: Weakening of the Walker circulation and apparent dominance of El Niño both reach record levels, but has ENSO really changed? *Geophys. Res. Lett.,* **34,** L18702, doi:10.1029/2007GL030854.

——, and G. Kociuba, 2011: What caused the observed twentieth-century weakening of the Walker circulation? *J. Climate,* **24,** 6501–6514.

Rayner, N. A., and Coauthors, 2003: Global analyses of sea surface temperature, sea ice, and night marine air temperature since the late nineteenth century. *J. Geophys. Res.,* **108,** 4407, doi:10.1029/2002JD002670.

Rodgers, K. B., P. Friederichs, and M. Latif, 2004: Tropical Pacific decadal variability and its relation to decadal modulation of ENSO. *J. Climate,* **17,** 3761–3774.

Smith, T. M., R. W. Reynolds, T. C. Peterson, and J. Lawrimore, 2008: Improvements to NOAA's historical merged land–ocean

surface temperature analysis (1880–2006). *J. Climate,* **21,** 2283–2296.

Tokinaga, H., S -P. Xie, C. Deser, Y. Kosaka, and Y. M. Okumura, 2012a: Slowdown of the Walker circulation driven by tropical Indo-Pacific warming. *Nature,* **491,** 439–443, doi:10.1038/nature11576.

——, ——, A. Timmermann, S. McGregor, T. Ogata, H. Kubota, and Y. M. Okumura, 2012b: Regional patterns of tropical Indo-Pacific climate change: Evidence of the Walker circulation weakening. *J. Climate,* **25,** 1689–1710.

Vecchi, G. A., and B. J. Soden, 2007: Global warming and the weakening of the tropical circulation. *J. Climate,* **20,** 4316–4340.

——, ——, A. T. Wittenberg, I. M. Held, A. Leetmaa, and M. J. Harrison, 2006: Weakening of tropical Pacific atmospheric circulation due to anthropogenic forcing. *Nature,* **441,** 73–76, doi:10.1038/nature04744.

——, A. Clement, and B. J. Soden, 2008: Examining the tropical Pacific's response to global warming. *Eos, Trans. Amer. Geophys. Union,* **89,** 81–83.

Vimont, D. J., 2005: The contribution of the interannual ENSO cycle to the spatial pattern of decadal ENSO-like variability. *J. Climate,* **18,** 2080–2092.

Wentz, F. J., L. Ricciardulli, K. Hilburn, and C. Mears, 2007: How much more rain will global warming bring? *Science,* **317,** 233–235.

Zhang, M., and H. Song, 2006: Evidence of deceleration of atmospheric vertical overturning circulation over the tropical Pacific. *Geophys. Res. Lett.,* **33,** L12701, doi:10.1029/2006GL025942.